AMERICAN SOCIETY FOR MICROBIOLOGY | Infection and Immunity

Host-Microbial Interactions | Full-Length Text

Mycobacterium tuberculosis infection drives differential responses in the bone marrow hematopoietic stem and progenitor cells

Suhas Bobba,[1] Nicole C. Howard,[1] Shibali Das,[1] Mushtaq Ahmed,[2] Nargis Khan,[3,4,5] Ignacio Marchante,[6] Luis B. Barreiro,[7] Joaquin Sanz,[6] Maziar Divangahi,[3,4,5] Shabaana A. Khader[2]

AUTHOR AFFILIATIONS See affiliation list on p. 11.

ABSTRACT Hematopoietic stem and progenitor cells (HSPCs) play a vital role in the host response to infection through the rapid and robust production of mature immune cells. These HSPC responses can be influenced, directly and indirectly, by pathogens as well. Infection with *Mycobacterium tuberculosis* (*Mtb*) can drive lymphopoiesis through modulation of type I interferon (IFN) signaling. We have previously found that the presence of a drug resistance (DR)-conferring mutation in *Mtb* drives altered host-pathogen interactions and heightened type I IFN production *in vitro*. But the impacts of this DR mutation on *in vivo* host responses to *Mtb* infection, particularly the hematopoietic compartment, remain unexplored. Using a mouse model, we show that, while drug-sensitive *Mtb* infection induces expansion of HSPC subsets and a skew toward lymphopoiesis, DR *Mtb* infection fails to induce an expansion of these subsets and an accumulation of mature granulocytes in the bone marrow. Using single-cell RNA sequencing, we show that the HSCs from DR *Mtb*-infected mice fail to upregulate pathways related to cytokine signaling across all profiled HSC subsets. Collectively, our studies report a novel finding of a chronic infection that fails to induce a potent hematopoietic response that can be further investigated to understand pathogen-host interaction at the level of hematopoiesis.

KEYWORDS hematopoiesis, *Mycobacterium tuberculosis*, infectious disease, stem cells

The host response to infection is a dynamic process that requires the generation and subsequent migration of mature immune cells to the site of infection to contain and eliminate the invading pathogen. Hematopoietic stem and progenitor cells (HSPCs) in the bone marrow are sources of these infiltrating immune cells and will exit a dormant state to produce the leukocytes necessary for host defense (1, 2). HSPCs are primed by host inflammatory signals to produce immune cells in the necessary quantity and with optimal functionality as needed (3–5). However, these signaling mechanisms can be modulated by successful, virulent pathogens to alter hematopoiesis and limit the generation of protective immune cells (6–8). For example, *Mycobacterium tuberculosis (Mtb*), the causative agent of tuberculosis (TB), can disseminate and access the privileged bone marrow niche during aerosol infection (9, 10), and, through manipulation of host type I interferon (IFN) signaling, drive the death of myeloid progenitors and the production of macrophages that are limited in their ability to kill *Mtb* (6). While Khan et al. highlighted how the virulence of *Mtb* can be attributed to this underexplored immunomodulation in sites distal to infection, much of the work compared a laboratory-adapted *Mtb* strain, H37Rv, with an avirulent TB strain, *Mycobacterium bovis*. It still remains to be studied how pervasive these host-pathogen interactions are across *Mtb* strains and how they might be driven.

Editor Sabine Ehrt, Weill Cornell Medicine, New York, New York, USA

Address correspondence to Shabaana A. Khader, khader@uchicago.edu.

The authors declare no conflict of interest.

See the funding table on p. 12.

Received 30 May 2023
Accepted 16 August 2023
Published 27 September 2023

Using a clinically relevant and hypervirulent *Mtb* strain from the W-Beijing family (11, 12), HN878, we found that the presence of certain drug resistance (DR)-conferring mutations in *Mtb* alters host-pathogen interactions *in vitro* and *in vivo* (13). The presence of the H445Y DR mutation in *rpoB* but not other DR mutations, such as S450L, can heighten the production of type I IFNs, limit the production of interleukin-1 (IL-1), and bypass IL-1 protective immunity. As type I IFN signaling was shown to affect hematopoiesis during *Mtb* infection, we sought to characterize how two *Mtb* strains that can more potently induce type I IFN production than H37Rv, HN878, and H445Y affect the hematopoietic response to *Mtb* infection. While infection with the drug-sensitive *Mtb* strain drove expansions of HSCs and lymphopoiesis as well as a decline in the myeloid progenitor population, infection with the hyper-type I IFN-producing DR *Mtb* strain resulted in a limited expansion of HSCs and instead drove granulopoiesis. Analysis of the HSCs after infection with either strain with single-cell RNA sequencing (scRNA-Seq) revealed divergent transcriptional landscapes. HSCs following H445Y *Mtb* infection exhibited decreased responses to cytokine signaling, suggesting that the divergence in the HSC response between infections could be linked to insufficient activation of the HSCs. Thus, our results highlight how virulent *Mtb* strains can drive different hematopoietic responses to infection, even when the strains are both potent type I IFN inducers. These findings contribute to our understanding of HSPC responses to chronic infections and suggest new avenues to further study host-pathogen interactions and their impact on hematopoiesis.

RESULTS

Mtb strains differentially expand HSC populations

A recent study showed that infection with a laboratory-adapted *Mtb* strain, H37Rv, activates and expands HSPCs in the bone marrow (BM), prevents myelopoiesis, and biases HSPCs toward lymphopoiesis (6). Using a clinically relevant *Mtb* strain, HN878, and a drug-resistant strain generated from it, H445Y, we sought to investigate how different *Mtb* strains might impact HSPC behavior in the BM. We found that pulmonary infection of C57Bl/6 (B6) mice with HN878 *Mtb* or H445Y *Mtb* led to dissemination and accumulation of bacteria in the BM as early as 14 days post infection (dpi) and continued to accumulate during infection similarly (Fig. S1A). To characterize the stem cell and progenitor populations in the BM, we assessed the LKS+ (lineage negative, c-Kit+, Sca-1+) population, which includes the long-term HSCs (LT-HSCs) (LKS+, CD150+, CD48–), short-term HSCs (ST-HSCs) (LKS+, CD150+, CD48+), multipotent progenitors (MPPs) (LKS+, CD150–, CD48+), MPP3 (LKS+, CD150–, CD48+, CD34+, Flt3–), and MPP4 (LKS+, CD150–, CD48+, CD34+, Flt3+) (online supplementary file 1B). The myeloid progenitors were LK+ (lineage negative, c-Kit+, and Sca-1–) and included the common myeloid progenitors (CMPs) (LK+, CD16/32–, CD34+), the megakaryocyte and erythroid progenitors (MEPs) (LK+, CD16/32–, CD34–), and the granulocyte and monocyte progenitors (GMPs) (LK+, CD16/32+, CD34+). Additionally, the common lymphoid progenitors (CLPs) were lineage negative , c-Kit^{lo}, Sca-1^{lo}, and CD127+ (Fig. S1B).

We found that infection with HN878 *Mtb* resulted in an early increase in the absolute number of LKS+ cells in the BM, with further expansion, likely through proliferation, during later time points when compared to uninfected mice (Fig. 1A) (6). In contrast, while we observed an early expansion of LKS+ cells following H445Y *Mtb* infection, by 30 dpi, we saw a contraction of the population to numbers comparable to uninfected mice. Profiling the LKS populations more deeply, we quantified the numbers of various HSC subpopulations. While there was no significant change in the numbers of LT-HSCs throughout HN878 infection (Fig. 1B), we observed an increase in this cell type during H445Y *Mtb* infection. With regard to the ST-HSCs, both infections resulted in an increase in their number by 30 dpi (Fig. 1C). However, the ST-HSCs were far more expanded in the HN878 *Mtb* infection relative to H445Y *Mtb*. When we profiled the MPPs comprising MPP3 and MPP4 subpopulations, we observed a similar pattern. While there was expansion of the MPPs, notably in the MPP3s, during H445Y infection, there were far

more MPP3s following HN878 infection at 30 dpi (Fig. 1D and E). We also observed an early increase in the number of MPP4s during HN878 infection at 14 dpi that was lacking during H445Y infection (Fig. 1F). Together, our results suggest that H445Y *Mtb* infection fails to induce a sustained and large expansion of HSCs, unlike HN878 *Mtb* infection.

Mtb strains differentially affect downstream progenitor and mature immune cell populations

After observing the differences in the responses of the stem cell populations, we next profiled the progenitor populations that are more differentiated and limited in their self-renewal capacity than the HSCs. The host requires a drastic influx of lymphoid populations to respond to *Mtb* infection, as adaptive immunity is critically required to control *Mtb* bacterial replication (14–17). As such, *Mtb* infection was reported to drive increases in the CLP population (6). We observed that infection with HN878 *Mtb* led to an early and sustained expansion of the CLPs (Fig. 2A). In contrast, we found that H445Y *Mtb* infection expanded the CLPs early at 14 dpi, but this response failed to continue at 30 dpi. Conversely, *Mtb* infection was reported to drive the cell death of CMPs through disruptions in iron metabolism, mediated through type I IFN signaling (6). In our infection model using HN878 *Mtb*, we also observed a decline in the numbers of CMPs at 30 dpi (Fig. 2B). However, infection with H445Y *Mtb* did not impact the numbers of CMPs, and the population appeared to be relatively stable across the observed time points. CMPs differentiate into more committed progenitors like MEPs, which give rise to erythrocytes or megakaryocytes, and GMPs, which are crucial in the generation of mature granulocyte and monocyte populations. Similar to the number of CMPs, the number of MEPs also declined during HN878 *Mtb* infection at the same time point, while the numbers of MEPs did not change during H445Y *Mtb* infection (Fig. 2D). As has been reported with aerosolized H37Rv *Mtb* infection, we did not find any differences

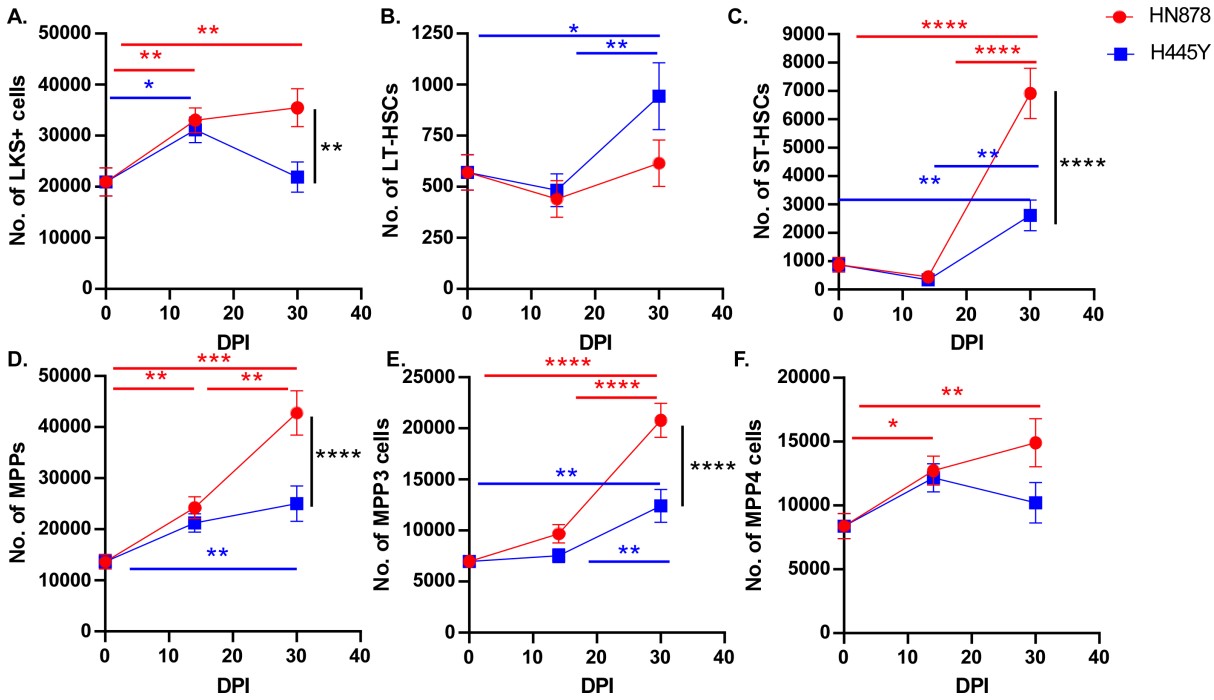

FIG 1 H445Y *Mtb* infection shows limited expansion of HSC populations. B6 mice were aerosol-infected with a low aerosol dose of HN878 or H445Y *Mtb* and sacrificed at the indicated time points. Bone marrow was collected from the hind legs, processed into single-cell suspensions, and stained for flow cytometry. The numbers of (A) LKS^+ cells (lineage negative, c-Kit positive, Sca1 positive), (B) LT-HSCs, (C) ST-HSCs, (D) MPP cells, (E) MPP3 cells, and (F) MPP4 cells in the bone marrow of infected and uninfected mice were determined by flow cytometry. The data shown represent the mean ± SEM of six to eight biological replicates per experiment. Significant differences are indicated with asterisks (*, $P < 0.05$; **, $P < 0.01$; ***, $P < 0.001$; and ****, $P < 0.0001$) by a two-way analysis of variance with Tukey's multiple comparisons tests. One of three independent experiments shown.

in the numbers of GMPs following HN878 *Mtb* infection (Fig. 2C). On the other hand, we found an increase in the number of GMPs at 30 dpi with H445Y *Mtb*. These data collectively indicate that HN878 and H445Y *Mtb* infections drive different kinetics in the accumulation of progenitor populations.

Following an analysis of the numbers of HSPCs in the bone marrow, we then studied the impact of the changes in these populations on the mature myeloid cell output. Using the outlined gating strategy, we quantified the numbers of neutrophils, monocytes, and CD11b$^+$ Gr1 cells (consisting of macrophages and some DC populations) in the bone marrow (Fig. 3A). While the numbers of neutrophils did not change over the course of HN878 *Mtb* infection, we found a significant accumulation in the absolute numbers of neutrophils, whether through increased production or decreased egress from the bone marrow, at 30 days following H445Y *Mtb* infection, relative to HN878 *Mtb*-infected and uninfected mice (Fig. 3B). With regard to monocytes, we found fewer numbers of them at 14 days after H445Y *Mtb* infection relative to HN878 *Mtb* infection (Fig. 3C). But this population then significantly increased by 30 days post H445Y *Mtb* infection and was found in greater numbers in the bone marrow than during HN878 *Mtb* infection at the same time point. We observed a similar pattern of monocyte accumulation in the numbers of CD11b$^+$ Gr1 cells during H445Y *Mtb* infection (Fig. 3D). In contrast, the numbers of this cell type decreased during HN878 *Mtb* infection after 30 days. The accumulation of these mature myeloid cells in the bone marrow during H445Y *Mtb*

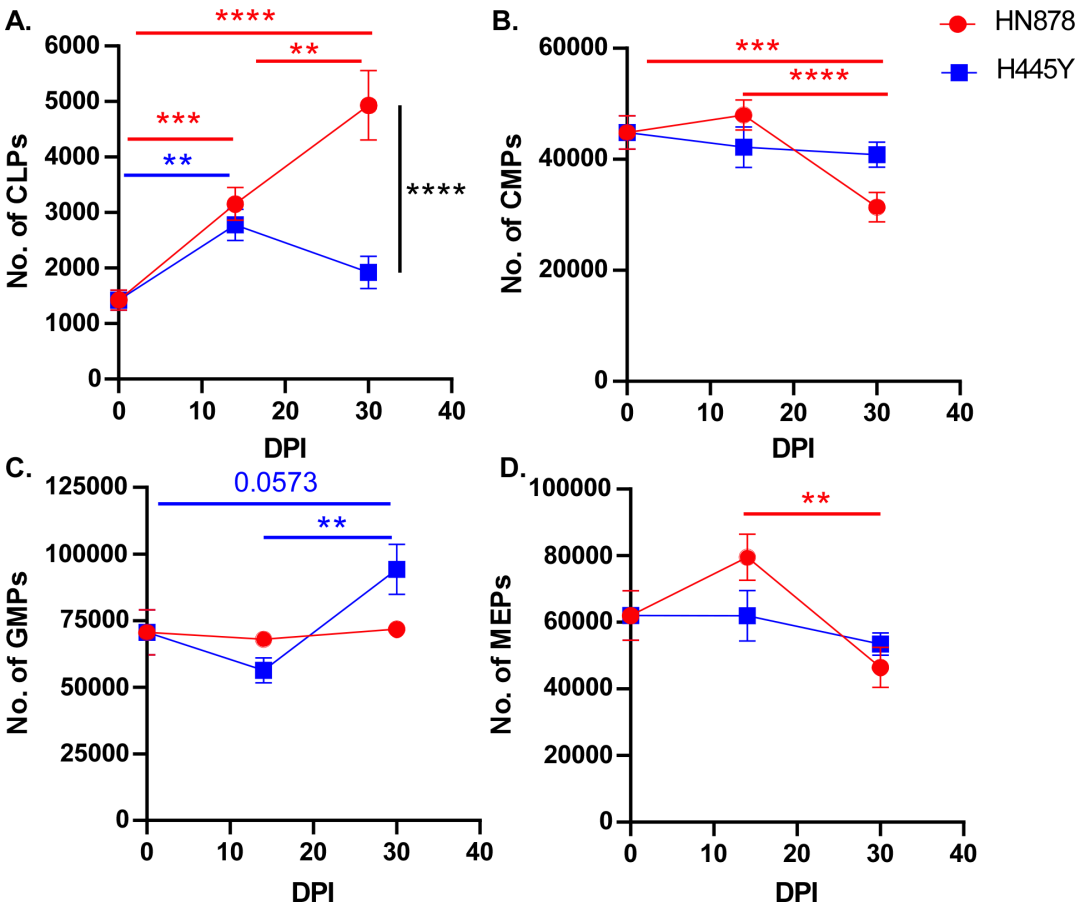

FIG 2 H445Y *Mtb* infection drives differential kinetics in progenitor populations. B6 mice were aerosol-infected with a low aerosol dose of HN878 or H445Y *Mtb* and sacrificed at the indicated time points. Bone marrow was collected from the hind legs, processed into single-cell suspensions, and stained for flow cytometry. The numbers of (A) CLPs, (B) CMPs, (C) GMPs, and (D) MEPs in the bone marrow of infected and uninfected mice were determined by flow cytometry. The data shown represent the mean ± SEM of six to eight biological replicates per experiment. Significant differences are indicated with asterisks (**, $P < 0.01$; ***, $P < 0.001$; and ****, $P < 0.0001$) by a two-way analysis of variance with Tukey's multiple comparisons tests. One of three independent experiments shown.

infection correlated with the expansion of the GMPs at the same time point. Together, these data highlight how HN878 *Mtb* and H445Y *Mtb* infections can drive the expansion and accumulation of different progenitor and mature cell populations, respectively.

LKS populations exhibit transcriptional differences between *Mtb* infections

To further elucidate the HSC response to infection, we performed scRNA-seq on isolated LKS+ cells from the BM of mice infected with either Wt HN878 or H445Y *Mtb* at 30 dpi and compared responses with those of uninfected mice (Fig. 4A). Based on canonical markers and differentially expressed genes, HSCs or MPP clusters were identified (Fig. 4B) in proportions largely comparable across samples (Fig. 4C). As expected, both Wt HN878 and H445Y *Mtb* infections led to significant changes in the gene expression of hundreds of genes in LT-HSCs, ST-HSCs, MPP3, and MPP4 populations (Fig. 4D). However, the nature of the response between the two *Mtb* strains appeared to be significantly different. For example, genes involved in cytokine signaling pathways, including tumor necrosis factor alpha (TNFa), both type I and II IFNs, and IL-6, were upregulated across several clusters after Wt HN878 infection but not rpoB-H445Y in comparison with uninfected mice (Fig.

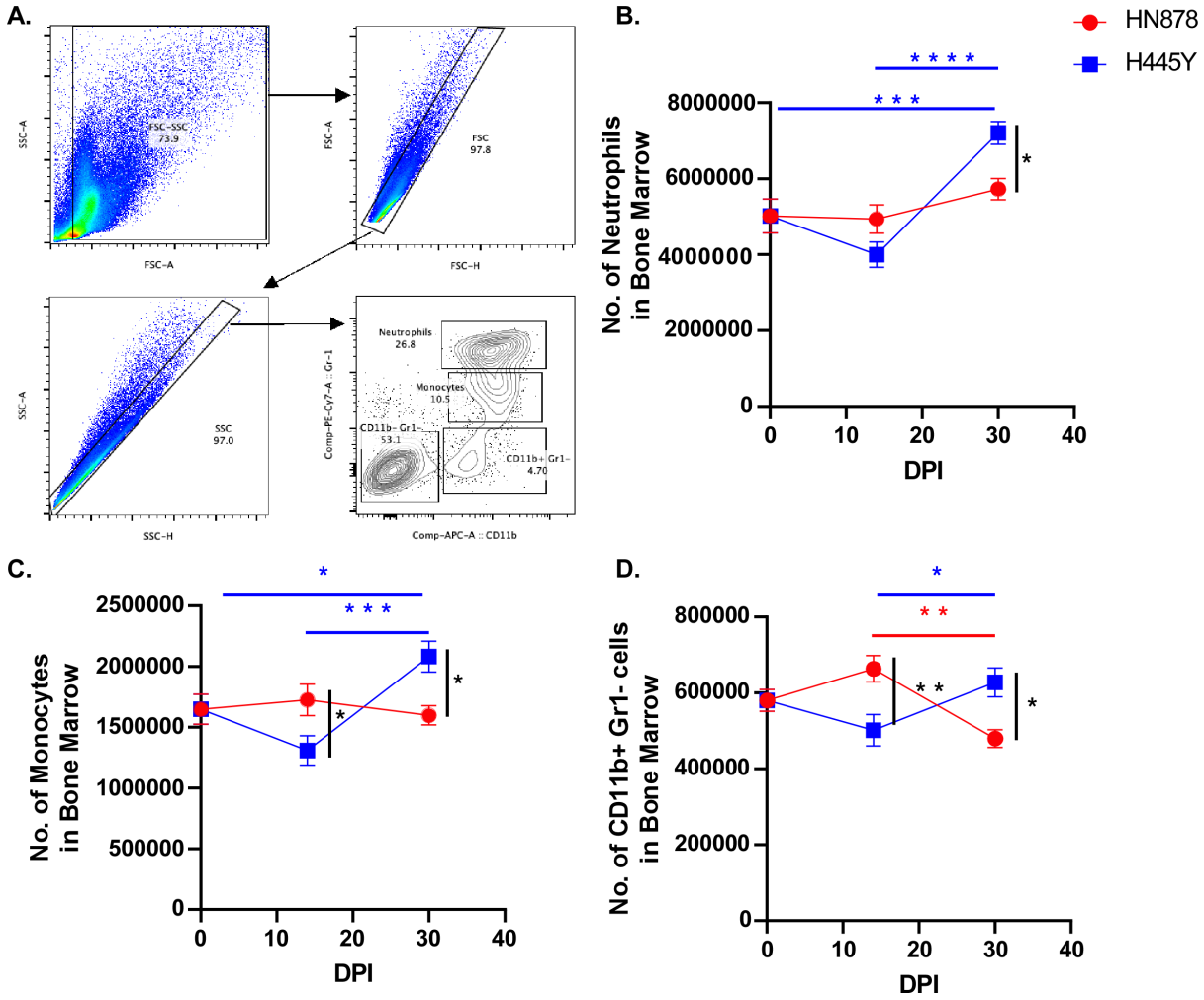

FIG 3 H445Y *Mtb* infection drives the accumulation of mature myeloid populations. B6 mice were aerosol-infected with a low dose of HN878 or H445Y *Mtb* and sacrificed at the indicated time points. Bone marrow was collected from the hind legs, processed into single-cell suspensions, and stained for flow cytometry. (A) The gating strategy for the identification of mature myeloid populations is shown. The numbers of (B) neutrophils ($CD11b^+$ $Gr1^{hi}$), (C) monocytes ($CD11c^+$ $Gr1^{int}$), and (D) $CD11b^+$ $Gr1^-$ cells in the bone marrow of infected and uninfected mice were determined by flow cytometry. The data shown represent the mean ± SEM of seven to eight biological replicates per experiment. Significant differences are indicated with asterisks (*, $P < 0.05$; **, $P < 0.01$; ***, $P < 0.001$; and ****, $P < 0.0001$) by a two-way analysis of variance with Tukey's multiple comparisons tests. One of two independent experiments shown.

4E, left and middle heatmaps). Indeed, all of the profiled cytokine signaling pathways were downregulated in H445Y infection when compared with HN878 *Mtb* infection (Fig. 4E, right heatmap). In addition, the expression of key downstream mediators of cytokine signaling, like *Junb*, is decreased in H445Y infection relative to HN878 Mtb infection (Fig. 4F). *Junb* inactivation has been shown to result in increased LT-HSC proliferation and dysregulated hematopoiesis, leading to an increase in myeloid differentiation (18). These results, in conjunction with the roles of cytokine signaling in promoting proliferation and differentiation (4, 5, 19, 20), suggest that the lack of expansion in HSPC subsets and the accumulation of myeloid cells following H445Y *Mtb* infection could be due to a limited cytokine response and downregulation of *Junb*.

DISCUSSION

Hematopoiesis is a crucial component of the host immune response to infection (1, 2). Whether the host requires an emergency response to an acute infection or a sustained production of immune cells for chronic insult, HSPCs will give rise to the necessary leukocytes to mount an effective immune response (21, 22). While substantial efforts have been made to uncover the processes by which short-term inflammation and signaling shape HSPC behavior, responses to chronic illness remain understudied. Although recent work has shed light on how *Mtb* can impact HSPCs during long-term infection, we sought to further study how different *Mtb* strains with drug resistance mutations might shape HSPC dynamics. In this work, we show how two closely related *Mtb* strains can drive diverging hematopoietic programs during infection. HN878 *Mtb* infection resulted in expanding HSCs and promoting lymphopoiesis, and H445Y *Mtb* infection drove granulopoiesis, with an increase in the numbers of GMPs and mature granulocytes and monocytes. Moreover, HSCs that were not expanding during H445Y

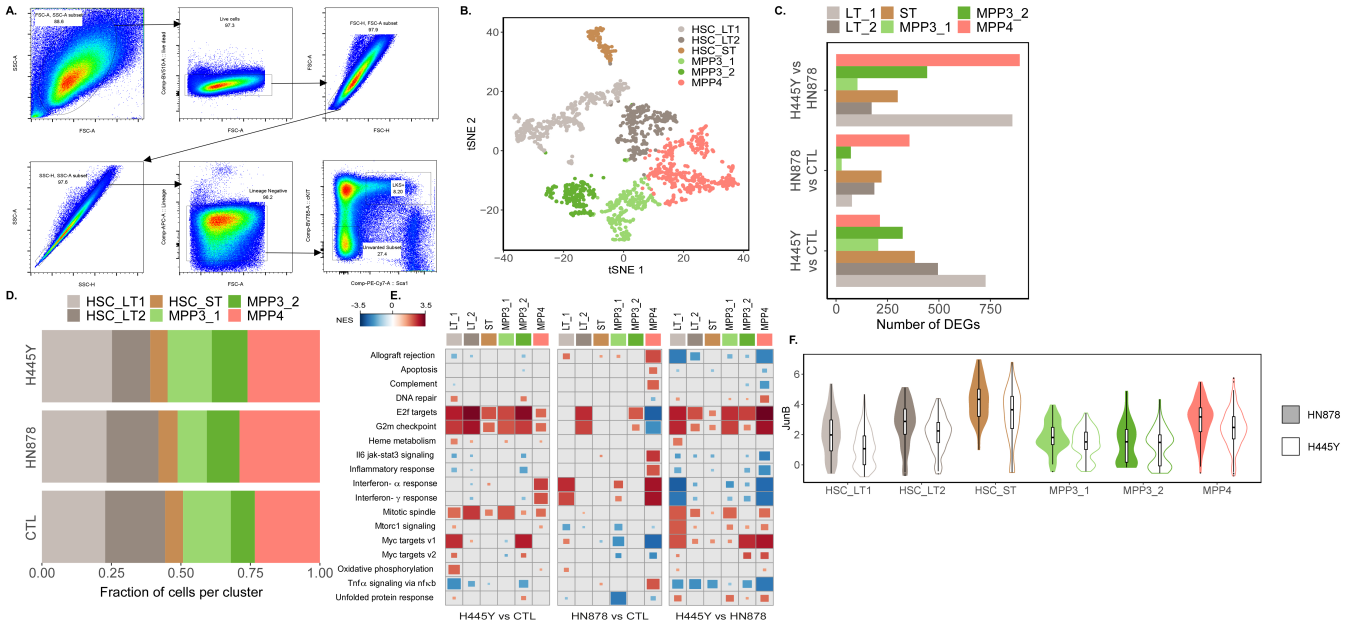

FIG 4 H445Y *Mtb* infection does not trigger cytokine signaling pathways in HSCs. B6 mice were aerosol-infected with a low dose of HN878 or H445Y *Mtb*. (A) A gating strategy for sorting LKS$^+$ cells from the BM is shown. (B) t-Distributed stochastic neighbor embedding plot of LKS$^+$ cells across all samples, colored according to identified clusters. (C) Proportion of each cluster type across conditions. (D) Numbers of differentially expressed genes in each cluster when comparing various conditions. (E) Heatmap of normalized enrichment scores of gene set enrichment analysis of differentially expressed genes in each cluster per condition. The gene sets included in the panel are those showing an enrichment with false discovery rate (FDR) = 1E−6 or lower for at least one of those contrasts explored in at least one cluster. Tiles are included for enrichments significant under FDR = 0.05 in each case, and their size is proportional to the −log10(FDR) of the associated enrichments (the most significant FDR, corresponding to a full tile, corresponds to FDR <5E−15). (F) Violin plots comparing the fold expression of *Junb* across identified clusters for HN878 and H445Y conditions over the uninfected controls. Significant differences in expression levels between the strains were observed for all clusters except MPP3_1 and MPP3_2.

Mtb infection exhibit decreased responsiveness to cytokine signaling. Taken together, our findings suggest that chronic virulent *Mtb* infection can result in different hematopoietic responses in the bone marrow, which can have consequences for long-term immunity.

There are a few ways to interpret the HSPC response to the H445Y *Mtb* infection. For many of the HSPC subsets, like the LKS+ cells and the CLPs, H445Y *Mtb* infection appears to drive similar responses to HN878 *Mtb* infection early in infection. However, by 30 dpi, these populations appear to either contract or stop expanding and are much smaller than their counterparts during the HN878 *Mtb* infection. These observations suggest that there might be a point between 14 and 30 dpi where the behavior of these cells is altered. Whether this change is caused by differences in host signaling, bacterial effectors, or other processes remains to be studied. From the scRNA-Seq data set, we observe a lack of cytokine signaling across various signaling pathways, suggesting that there might be a master regulator non-specifically governing the response to these various interferons and interleukins. Unexpectedly, the upregulated pathways in the HSCs following H445Y *Mtb* infection are related to cell cycle pathways, such as E2F targets and the G2M checkpoint. Enrichment of genes in these pathways would indicate actively dividing cells, but these HSC populations during H445Y *Mtb* infection are all smaller than their counterparts after HN878 *Mtb* infection. This discrepancy between transcription and hematopoiesis remains to be bridged. With the number of mice used per condition, we are limited in commenting on the reproducibility of these transcriptional differences across sample sizes, but from the design of the scRNA-Seq analysis, we observed robust differences.

When comparing the HSPC responses between our findings and previously published results, we found that aerosol infection with HN878 *Mtb* largely mirrors aerosol infection with H37Rv *Mtb*. However, we do see some changes in the kinetics of these responses. The increase in the number of CLPs and the decrease in the number of CMPs occur more rapidly during HN878 *Mtb* infection. This difference in the timeframe of the HSPC response could be attributed to a number of factors, from the virulence of the *Mtb* strain to subtler differences regarding microbiota (23) and rearing across separate institutions. While the kinetics could also be affected by the rate of dissemination of bacteria to the bone marrow, as seen comparing intravenous and aerosol infections (6), we observed similar dissemination between the HN878 *Mtb* infection and previously published results with H37Rv *Mtb*. An ultra-low dose model with heterogenous dissemination of *Mtb* could further explore this relationship (24). It is also important to note that HN878 *Mtb* is a more potent inducer of type I IFN than the H37Rv strain (25). While a faster contraction of the CMP population during HN878 *Mtb* infection could be correlated with a greater production of type I IFNs, the lack of change in CMP numbers during H445Y *Mtb* infection, a strain we have observed to drive even greater production of type I IFNs (13), suggests that this is not exactly a linear relationship. Furthermore, type I IFN signaling has not been shown to impact CLP expansion during infection of *Ifnar*$^{-/-}$ mice with H37Rv *Mtb* (6). A deeper examination of the role of type I IFN signaling in these responses and how that signal is propagated in the bone marrow niche relative to the lung microenvironment is necessary. An important area of emerging study in the cross-section of hematopoiesis and infection is immune memory. In addition to affecting short-term immune cell production, *Mtb* has been shown to leave lasting effects on the host post TB treatment in the form of epigenetic changes on HSCs termed trained immunity (3, 6, 26–28). While we were limited in our ability to treat drug-resistant *Mtb* infection, it would be interesting to study if the differences in the hematopoietic responses to infection with these strains would also have impacts on long-term trained immunity following potential resolution of infection. Thus, our work opens up several avenues for future study.

A major question that is raised in our study is the role of the pathogen and its associated virulence factors in driving differing HSPC responses. We isolated the DR H445Y *Mtb* strain from selective screening of the drug-sensitive (DS) HN878 *Mtb* strain

on antibiotic-containing media. So, in addition to the drug resistance-conferring H445Y single nucleotide polymorphism (SNP) in the RNA polymerase B subunit (*rpoB*), there exist a few other SNPs that distinguish the HN878 *Mtb* strain from the H445Y *Mtb* strain. Therefore, we cannot infer causality between the DR SNP and the phenotypes observed in the study, which must be confirmed in follow-up work. However, the finding that only a few SNPs separate HN878 and H445Y *Mtb* strains and result in significant HSPC responses during infection is still compelling and remains to be understood. We suggest that the location and identity of the DR SNP in *rpoB* could result in significant transcriptional changes for the pathogen, including major virulence factors (29). We have previously observed that the presence of the *rpoB*-H445Y SNP was associated with an increased abundance of long-chained phthiocerol dimycocerosate (PDIM), a mycobacterial cell wall lipid, in the cell wall of the DR *Mtb* when compared with the parental DS *Mtb* strain (13). PDIM has been shown to impact phagosome integrity and influence mycobacterial containment in macrophages (30). At the same time, some strains, such as the non-Beijing H37Rv strain, have been shown to spontaneously lose the ability to produce PDIM (31). How this cell wall lipid and other differentially regulated virulence factors between a DS strain and a DR strain with the *rpoB*-H445Y SNP in Beijing as well as non-Beijing families could impact the sensing and response of the HSPCs in the bone marrow niche and contribute to differences in virulence in patients remains to be studied.

In summary, our studies have shown heterogeneity in bone marrow hematopoietic responses to *Mtb* infection. These differences underscore the need to extensively study hematopoiesis in the context of chronic infection and inflammation, with a special emphasis on the kinetics of these processes. Investigating these host-pathogen interactions can reveal novel pathways that could be leveraged to develop effective host-directed therapeutics.

MATERIALS AND METHODS

Mice

C57BL/6J (B6) mice on the B6 background were purchased from The Jackson Laboratory (Bar Harbor, ME, USA). All mice were maintained in the animal facility at Washington University in St. Louis and bred in-house. Experimental mice were age- and sex-matched and infected between the ages of 6 and 8 weeks. All mice were maintained and used in accordance with the approved Washington University in St. Louis Institutional Animal Care and Use Committee guidelines.

Mtb infections

Mtb strain HN878 was obtained from BEI resources (Manassas, VA, USA) under National Institutes of Health contract AI-75320. Independent rifampicin-resistant *Mtb* HN878 colonies (biological replicates) were selected from rifampicin (2 µg/mL)-containing 7H11 agar plates (32). The sequences of *rpoB* were confirmed by Sanger sequencing (Genewiz), and *Mtb* stocks were created for further experimentation. All *Mtb* strains were cultured in Proskauer Beck medium supplemented with 0.05% Tween 80 and frozen at −80°C while in the mid-log phase. Colony-forming units (CFU) of the bacterial stocks were determined through serial dilutions on 7H11 agar plates. Mice were aerosol-infected with low doses (~100 CFU) of indicated *Mtb* strains in sterile phosphate-buffered saline using a Glass-Col nebulizer (33). *Mtb* bacterial burden per organ was quantitated by plating aspirated bone marrow on 7H11 agar plates (BD Biosciences, Franklin Lakes, NJ, USA). Plates were incubated for 2–3 weeks at 37°C, and the number of colonies was counted.

Flow cytometry

BM was harvested from both femurs and tibiae and lysed for RBCs. BM cells were then stained with LIVE/DEAD fixable viability dye (Thermofisher), followed by staining with appropriate fluorochrome-labeled specific antibodies, including lineage markers [CD3 (145-2C11; BD Biosciences), CD5 (53-7.3; BioLegend), TER119 (TER-119; BD Biosciences), CD11b (M1/70; Tonbo Biosciences), Gr-1 (RB6-8C5; BD Biosciences), CD45R (RA3-6B2; BD Biosciences)], cKit (2B8; Invitrogen), Sca1 (D7; Invitrogen), CD34 (RAM34; Invitrogen), CD150 (mShad150; Invitrogen), CD48 (HM48-1; Invitrogen), Flt3 (A2F10; Invitrogen), CD16/CD32 (93; Invitrogen), CD127 (SB/199; BioLegend), and streptavidin (BD Biosciences).

Cells were processed with the Becton Dickinson (BD) Fortessa X-20 flow cytometer using FACS Diva software or the BD FACSJazz flow cytometer using FACS software (BD). Flow cytometry experiments were analyzed using FlowJo (Tree Star Inc.). The gating strategies for HSPC and myeloid populations in the bone marrow are shown in Fig. S1; Fig. 3, respectively (6). Total numbers of cells within each gate were back-calculated based on cell counts and individual samples.

LKS$^+$ cells sorting

LKS$^+$ populations were sorted from mice infected with either *rpoB*-H445Y *Mtb* or HN878 *Wt Mtb* as well as uninfected mice. Then, 30 days after infection, mice were sacrificed. BM cells were harvested and stained as previously described, using the following antibodies from the Lineage Depletion Kit according to the manufacturer's instructions (Miltenyi Biotec): lineage markers (CD3, CD5, Thy1.1, TER119, CD11b, Gr-1, and CD45R), LIVE/DEAD viability dye as above, cKit, and Sca1. To isolate the LKS$^+$ population, the Lin$^-$cKit$^+$Sca1$^+$ cells were sorted using the BD FACSJazz flow cytometer with FACS Sortware software, as outlined in Fig. 4A (BD). Cells were collected into phosphate-buffered saline containing 0.04% non-acetylated bovine serum albumin.

scRNA-seq library generation

scRNA-seq was done according to the manufacturer's instructions (10× genomics) as before (34). Sorted LKS$^+$ single-cell suspensions were subjected to droplet-based massively parallel scRNA-seq using the Chromium Single Cell 3′ (v3) Reagent Kit in the BSL-3 laboratory as per the manufacturer's instructions (10× genomics). Briefly, cell suspensions were loaded at 1,000 cells/µL to capture 10,000 cells/lane. The 10× Chromium Controller generated GEM droplets, where each cell was labeled with a specific barcode and each transcript was labeled with a unique molecular identifier (UMI) during reverse transcription. The barcoded cDNA was isolated and removed from the BSL-3 space for library generation. The cDNA underwent 11 cycles of amplification, followed by fragmentation, end repair, A-tailing, adaptor ligation, and sample index PCR as per the manufacturer's instructions. Libraries were sequenced on a NovaSeq S4 (200 cycles) flow cell, targeting 50,000 read pairs/cell.

scRNA-seq data preprocessing and quality control

Samples were processed using the count command in CellRanger and aligned against the mm10 1.2.0 mouse reference genome. A total of 18,046 genes were measured when combining data across all cells. Using this set of genes, we calculated the percentage of mitochondrial RNA per cell as well as the percentage of RNA coming from protein-coding genes. Cells that featured (i) a high fraction of mitochondrial RNA reads (f_{mito} §amp;gt; 10%) or a low percentage of protein-coding genes (f_{pc} §amp;lt; 90%) were excluded. We then explored the complexities of the libraries associated with each barcode and identified an additional subset of cells with lower complexity than the rest, which were also excluded [nUMI <2,500 or log(nGene) < 4.32 + 0.38·log(nUMI)]. Once the final set of cells is selected, genes detected in less than five of the surviving cells in all conditions, mitochondrial genes, as well as genes with biotypes different from protein

coding, are also removed. After the quality control (QC), our final data set included gene expression measurements for 12,909 genes across 1,596 cells in total.

scRNA-seq data normalization, scaling, and variance stabilization

All the scRNA-seq data treatments were done as previously described (6). Briefly, the data were normalized using the function computeSumFactors from the R package scran, which proposes a robust approach for normalization of scRNA-seq data that is suitable for comparisons across samples. The data were then log-transformed according to the following expression: $E_{norm}(i,j) = log_2(1 + E_{count}(i,j)/n_i)$, where the normalized expression estimates at sample *i* and gene *j* $E_{norm}(i,j)$ are obtained from the count abundances $E_{count}(i,j)$ and the normalization coefficients per sample n_i . Then, the normalized expression levels were modeled according to a linear model: $E \sim f_{pc} + f_{mito} + n_{UMI} + C + \varepsilon$, where f_{pc}, f_{mito}, and n_{UMI} are the mean-centered and scaled fractions of protein-coding fragments, mitochondrial fragments, and numbers of UMIs per cell, respectively; and C is the cell-cycle score obtained using the scran function cyclone (35). After fitting the model, we extracted the residuals, which were then transformed to remove gene-wise heteroskedasticity as described before (6). Proceeding this way, we generate a version of the data set that has been (i) scaled (i.e., deprived of the effects of technical covariates from normalized gene expression) and (ii) variance-stabilized.

Sample integration, dimensionality reduction, and clustering

We further selected a set of highly informative genes as the intersection between genes showing high levels of biological variation across cells and those reported in previous works (3, 6) as differential expression markers between the subtypes of LKS cells present in the samples. Using these genes, we first integrated the data across samples using the anchoring routine proposed in Seurat (FindIntegrationAnchors). After data integration, the steps of scaling and identification of highly informative genes were repeated on the integrated data, as previously described (6). The expression estimates of the highly informative genes in the integrated, scaled, and variance-stabilized version of the data set were then used to conduct dimensionality reduction: principal component analysis and t-distributed stochastic neighbor embedding. Finally, using the first 20 principal components at a resolution of 0.15, the Seurat routines FindNeighbors and FindClusters were used to identify the six clusters reported in this work, whose identities were proposed upon inspection of the patterns of the averages of gene expression levels of genes reported to be differentially expressed (i) between MPPs and HSCs, (ii) between MPP3s and MPP4s within MPPs, and (iii) between long-term and short-term HSCs.

Differential expression and gene set enrichment analysis

Finally, we interrogated the differences in expression of genes in response to H445Y or HN878 challenges, as well as the differences in expression between the samples infected with Wt and RDR *Mtb*. To conduct these analyses, normalized (though not scaled or integrated) data were used under the following experimental design:

$$E \sim f_{pc} + f_{mito} + n_{UMI} + Cluster + Condition{:}Cluster + \varepsilon$$

Finally, gene set enrichment analyses were carried out using the R package fgsea (36). To that end, ranks of standardized differences in expression between the three conditions present in the study were retrieved in each of the clusters identified and interrogated for enrichments within those ranks of genesets in a mouse version of the hallmark geneset collection from the molecular signatures database MdigDB (http://bioinf.wehi.edu.au/MSigDB/, based on MSigDB version 7.1, org.Mm.eg.db version 3.11.4, and NCBI gene information file dated 12 June 2020).

Statistical analysis

All data sets were evaluated for normality using the Shapiro-Wilk test. Differences between the means of groups were analyzed using either the two-tailed Student's *t*-test or the Mann-Whitney test, where applicable. Differences between the means of more than two groups were analyzed using one-way analysis of variance (ANOVA) or two-way ANOVA for time course studies, with Tukey's post tests for normally distributed distributions or the Kruskal-Wallis test with Dunn's multiple comparisons tests. All statistical analyses were done in GraphPad Prism 9. A P value of <0.05 was considered significant. The data points across figures represent the mean (±SD or ±SEM) of values, as noted. *, $P \leq 0.05$; **, $P \leq 0.01$; ***, $P \leq 0.001$; ****, $P \leq 0.0001$; ns, not significant ($P > 0.05$). All experiments were replicated for reproducibility.

Study approval

Protocols involving the use of animals were approved by the IACUC at Washington University in St. Louis. All of the experiments were performed in accordance with the protocols.

ACKNOWLEDGMENTS

We thank Mr. Andrew Beckendorf, Ms. Lan Lu, and Ms. Misty Veschak for technical support. We thank the Genome Technology Access Center at the McDonnell Genome Institute at Washington University School of Medicine for helping with genomics services. The Center is partially supported by NCI Cancer Center Support Grant #P30 CA91842 to the Siteman Cancer Center and by ICTS/CTSA Grant #UL1TR002345 from the National Center for Research Resources (NCRR), a component of the National Institutes of Health (NIH), and the NIH Roadmap for Medical Research. This publication is solely the responsibility of the authors and does not necessarily represent the official view of NCRR or NIH.

This work was supported by Washington University School of Medicine, NIH grants HL105427, AI111914-02, AI134236-02, and AI123780 to S.A.K. and NIH/NHLBI T32 HL007317-44 to S.B. J.S. and I.M. were supported by grants RYC-2017-23560 and PID2019-106859GA-I00 funded by MCIN/AEI/ 10.13039/501100011033 and by "ESF Investing in Your Future."

S.A.K. designed the study, provided funding, and supervised the project. S.B., N.C.H., S.D., and M.A. performed the experiments and compiled the results. I.M., J.S., and L.B. performed the scRNA-Seq analysis, comparative transcriptomics, and functional enrichment analysis. S.B., N.C.H., N.K., I.M., J.S., L.B., M.D., and S.A.K. interpreted the experiments, carried out the data analysis, and/or provided the reagents. S.B. and S.A.K. wrote the manuscript; all authors edited and approved the final version of the manuscript.

The authors have declared that no conflict of interest exists.

AUTHOR AFFILIATIONS

[1]Department of Molecular Microbiology, Washington University School of Medicine, St. Louis, Missouri, USA
[2]Department of Microbiology, University of Chicago, Chicago, Illinois, USA
[3]Meakins-Christie Laboratories, Department of Medicine, McGill University, Montreal, Quebec, Canada
[4]Meakins-Christie Laboratories, Department of Microbiology and Immunology, McGill University, Montreal, Quebec, Canada
[5]Meakins-Christie Laboratories, Department of Pathology, McGill University, Montreal, Quebec, Canada
[6]Department of Theoretical Physics, University of Zaragoza, Institute for Biocomputation and Physics of Complex Systems (BIFI), Zaragoza, Spain

[7]Department of Medicine, Genetic Section, University of Chicago, Chicago, Illinois, USA

AUTHOR ORCIDs

Suhas Bobba http://orcid.org/0000-0002-9276-1469
Shabaana A. Khader http://orcid.org/0000-0002-9545-4982

FUNDING

Funder	Grant(s)	Author(s)
HHS | National Institutes of Health (NIH)	HL105427, AI111914-02, AI134236-02, AI123780	Shabaana A. Khader
HHS | NIH | National Heart, Lung, and Blood Institute (NHLBI)	T32 HL007317-42	Suhas Bobba
Ministerio de Ciencia e Innovación (MCIN)	RYC-2017-23560	Joaquin Sanz
ESF Investing in your future	PID2019-106859GA-I00	Joaquin Sanz

AUTHOR CONTRIBUTIONS

Suhas Bobba, Conceptualization, Formal analysis, Funding acquisition, Investigation, Methodology, Writing – original draft, Writing – review and editing | Nicole C. Howard, Conceptualization, Funding acquisition, Investigation, Writing – review and editing | Shibali Das, Formal analysis, Investigation, Writing – review and editing | Mushtaq Ahmed, Investigation, Writing – review and editing | Nargis Khan, Formal analysis, Methodology, Validation, Writing – review and editing | Ignacio Marchante, Data curation, Formal analysis, Funding acquisition, Methodology, Validation, Writing – review and editing, Software, Visualization | Luis B. Barreiro, Data curation, Formal analysis, Writing – review and editing | Joaquin Sanz, Data curation, Formal analysis, Funding acquisition, Methodology, Writing – review and editing, Software, Visualization | Maziar Divangahi, Formal analysis, Writing – review and editing | Shabaana A. Khader, Conceptualization, Formal analysis, Funding acquisition, Project administration, Resources, Supervision, Writing – review and editing

DATA AVAILABILITY

scRNA-seq data that support the findings of this study have been deposited in GEO (accession no. GSE176423). Other data that support the findings of this study are available from the corresponding author upon request.

ADDITIONAL FILES

The following material is available online.

Supplemental Material

Supplemental figure legend (IAI00201-23-S0001.docx). Legend for Fig S1.
Fig. S1 (IAI00201-23-S0002.tif). *Mycobacterium tuberculosis* (Mtb) travels to the bone marrow following infection.

REFERENCES

1. Baldridge MT, King KY, Goodell MA. 2011. Inflammatory signals regulate hematopoietic stem cells. Trends Immunol 32:57–65. https://doi.org/10.1016/j.it.2010.12.003
2. King KY, Goodell MA. 2011. Inflammatory modulation of hematopoietic stem cells: viewing the hematopoietic stem cell as a foundation for the immune response. Nat Rev Immunol 11:685–692.
3. Kaufmann E, Sanz J, Dunn JL, Khan N, Mendonça LE, Pacis A, Tzelepis F, Pernet E, Dumaine A, Grenier J-C, Mailhot-Léonard F, Ahmed E, Belle J, Besla R, Mazer B, King IL, Nijnik A, Robbins CS, Barreiro LB, Divangahi M. 2018. BCG Educates hematopoietic stem cells to generate protective innate immunity against tuberculosis. Cell 172:176–190. https://doi.org/10.1016/j.cell.2017.12.031

4. Essers MAG, Offner S, Blanco-Bose WE, Waibler Z, Kalinke U, Duchosal MA, Trumpp A. 2009. IFNα activates dormant haematopoietic stem cells in vivo. 7240. Nature 458:904–908. https://doi.org/10.1038/nature07815
5. Baldridge MT, King KY, Boles NC, Weksberg DC, Goodell MA. 2010. Quiescent haematopoietic stem cells are activated by IFN- in response to chronic infection. 7299. Nature 465:793–797. https://doi.org/10.1038/nature09135
6. Khan N, Downey J, Sanz J, Kaufmann E, Blankenhaus B, Pacis A, Pernet E, Ahmed E, Cardoso S, Nijnik A, Mazer B, Sassetti C, Behr MA, Soares MP, Barreiro LB, Divangahi M. 2020. *M. tuberculosis* reprograms hematopoietic stem cells to limit myelopoiesis and impair trained immunity. Cell 183:752–770. https://doi.org/10.1016/j.cell.2020.09.062
7. Katahira Y, Higuchi H, Matsushita H, Yahata T, Yamamoto Y, Koike R, Ando K, Sato K, Imadome K-I, Kotani A. 2019. Increased granulopoiesis in the bone marrow following epstein-barr virus infection. Sci Rep 9:13445. https://doi.org/10.1038/s41598-019-49937-w
8. Li F, Ma Y, Li X, Zhang D, Han J, Tan D, Mi Y, Yang X, Wang J, Zhu B. 2023. Severe persistent mycobacteria antigen stimulation causes lymphopenia through impairing hematopoiesis. Front Cell Infect Microbiol 13:1079774. https://doi.org/10.3389/fcimb.2023.1079774
9. Beamer G, Major S, Das B, Campos-Neto A. 2014. Bone marrow mesenchymal stem cells provide an antibiotic-protective niche for persistent viable *Mycobacterium tuberculosis* that survive antibiotic treatment. Am J Pathol 184:3170–3175. https://doi.org/10.1016/j.ajpath.2014.08.024
10. Das B, Kashino SS, Pulu I, Kalita D, Swami V, Yeger H, Felsher DW, Campos-Neto A. 2013. CD271+ bone marrow mesenchymal stem cells may provide a niche for dormant *Mycobacterium tuberculosis*. Sci Transl Med 5:170ra13. https://doi.org/10.1126/scitranslmed.3004912
11. Bifani PJ, Mathema B, Kurepina NE, Kreiswirth BN. 2002. Global dissemination of the *Mycobacterium tuberculosis* W-Beijing family strains. Trends Microbiol 10:45–52. https://doi.org/10.1016/s0966--842x(01)02277-6
12. Kremer K, Glynn JR, Lillebaek T, Niemann S, Kurepina NE, Kreiswirth BN, Bifani PJ, van Soolingen D. 2004. Definition of the Beijing/W lineage of *Mycobacterium tuberculosis* on the basis of genetic markers . J Clin Microbiol 42:4040–4049. https://doi.org/10.1128/JCM.42.9.4040-4049.2004
13. Howard NC, Marin ND, Ahmed M, Rosa BA, Martin J, Bambouskova M, Sergushichev A, Loginicheva E, Kurepina N, Rangel-Moreno J, Chen L, Kreiswirth BN, Klein RS, Balada-Llasat J-M, Torrelles JB, Amarasinghe GK, Mitreva M, Artyomov MN, Hsu F-F, Mathema B, Khader SA. 2018. *Mycobacterium tuberculosis* carrying a rifampicin drug resistance mutation reprograms macrophage metabolism through cell wall lipid changes. Nat Microbiol 3:1327. https://doi.org/10.1038/s41564-018-0281-9
14. Sakai S, Kauffman KD, Schenkel JM, McBerry CC, Mayer-Barber KD, Masopust D, Barber DL. 2014. Control of *Mycobacterium tuberculosis* infection by a subset of lung parenchyma homing CD4 T cells. J Immunol 192:2965–2969. https://doi.org/10.4049/jimmunol.1400019
15. Green AM, Difazio R, Flynn JL. 2013. IFN-Γ from CD4 T cells is essential for host survival and enhances CD8 T cell function during *Mycobacterium tuberculosis* Infectiony. J Immunol 190:270–277. https://doi.org/10.4049/jimmunol.1200061
16. Das S, Marin ND, Esaulova E, Ahmed M, Swain A, Rosa BA, Mitreva M, Rangel-Moreno J, Netea MG, Barreiro LB, Divangahi M, Artyomov MN, Kaushal D, Khader SA. 2021. Lung epithelial signaling mediates early vaccine-induced CD4+T cell activation and *Mtb* control. Immunology. https://doi.org/10.1101/2021.06.03.446981
17. Swanson RV, Gupta A, Foreman TW, Lu L, Choreno-Parra JA, Mbandi SK, Rosa BA, Akter S, Das S, Ahmed M, Garcia-Hernandez M de la L, Singh DK, Esaulova E, Artyomov MN, Gommerman J, Mehra S, Zuniga J, Mitreva M, Scriba TJ, Rangel-Moreno J, Kaushal D, Khader SA. 2023. Antigen-specific B cells direct T follicular-like helper cells into lymphoid follicles to mediate *Mycobacterium tuberculosis* control. Nat Immunol 24:855–868. https://doi.org/10.1038/s41590-023-01476-3
18. Santaguida M, Schepers K, King B, Sabnis AJ, Forsberg EC, Attema JL, Braun BS, Passegué E. 2009. JunB protects against myeloid malignancies by limiting hematopoietic stem cell proliferation and differentiation without affecting self-renewal. Cancer Cell 15:341–352. https://doi.org/10.1016/j.ccr.2009.02.016
19. Ehninger A, Boch T, Uckelmann H, Essers MA, Müdder K, Sleckman BP, Trumpp A. 2014. Posttranscriptional regulation of c-Myc expression in adult murine HSCs during homeostasis and interferon--induced stress response. Blood 123:3909–3913. https://doi.org/10.1182/blood-2013-10-531038
20. Yamashita M, Passegué E. 2019. TNFα coordinates hematopoietic stem cell survival and myeloid regeneration. Cell Stem Cell 25:357–372. https://doi.org/10.1016/j.stem.2019.05.019
21. Johnson CB, Zhang J, Lucas D. 2020. The role of the bone marrow microenvironment in the response to infection. Front Immunol 11:585402. https://doi.org/10.3389/fimmu.2020.585402
22. Collins A, Mitchell CA, Passegué E. 2021. Inflammatory signaling regulates hematopoietic stem and progenitor cell development and homeostasis. J Exp Med 218:e20201545. https://doi.org/10.1084/jem.20201545
23. Yan H, Walker FC, Ali A, Han H, Tan L, Veillon L, Lorenzi PL, Baldridge MT, King KY. 2022. The bacterial microbiota regulates normal hematopoiesis via metabolite-induced type 1 interferon signaling. Blood Adv 6:1754–1765. https://doi.org/10.1182/bloodadvances.2021006816
24. Plumlee CR, Duffy FJ, Gern BH, Delahaye JL, Cohen SB, Stoltzfus CR, Rustad TR, Hansen SG, Axthelm MK, Picker LJ, Aitchison JD, Sherman DR, Ganusov VV, Gerner MY, Zak DE, Urdahl KB. 2021. Ultra-low dose aerosol infection of mice with *Mycobacterium tuberculosis* more closely models human tuberculosis. Cell Host Microbe 29:68–82. https://doi.org/10.1016/j.chom.2020.10.003
25. Manca C, Tsenova L, Freeman S, Barczak AK, Tovey M, Murray PJ, Barry C, Kaplan G. 2005. Hypervirulent *M. tuberculosis* W/Beijing strains upregulate type 1 IFNs and increase expression of negative regulators of the jak-stat pathway. J Interferon Cytokine Res 25:694–701. https://doi.org/10.1089/jir.2005.25.694
26. Moorlag SJCFM, Khan N, Novakovic B, Kaufmann E, Jansen T, van Crevel R, Divangahi M, Netea MG. 2020. ß-Glucan induces protective trained immunity against *Mycobacterium tuberculosis* infection: a key role for IL-1. Cell Rep 31:107634. https://doi.org/10.1016/j.celrep.2020.107634
27. Penkov S, Mitroulis I, Hajishengallis G, Chavakis T. 2019. Immunometabolic crosstalk: an ancestral principle of trained immunity? Trends Immunol 40:1–11. https://doi.org/10.1016/j.it.2018.11.002
28. Netea MG, Domínguez-Andrés J, Barreiro LB, Chavakis T, Divangahi M, Fuchs E, Joosten LAB, van der Meer JWM, Mhlanga MM, Mulder WJM, Riksen NP, Schlitzer A, Schultze JL, Stabell Benn C, Sun JC, Xavier RJ, Latz E. 2020. Defining trained immunity and its role in health and disease. Nat Rev Immunol 20:375–388. https://doi.org/10.1038/s41577-020-0285-6
29. Lahiri N, Shah RR, Layre E, Young D, Ford C, Murray MB, Fortune SM, Moody DB. 2016. Rifampin resistance mutations are associated with broad chemical remodeling of *Mycobacterium tuberculosis*. J Biol Chem 291:14248–14256. https://doi.org/10.1074/jbc.M116.716704
30. Quigley J, Hughitt VK, Velikovsky CA, Mariuzza RA, El-Sayed NM, Briken V, Kaufmann SHE. 2017. The cell wall lipid PDIM contributes to phagosomal escape and host cell exit of *Mycobacterium tuberculosis* . mBio 8:mBio https://doi.org/10.1128/mBio.00148-17
31. Domenech P, Reed MB. 2009. Rapid and spontaneous loss of phthiocerol dimycocerosate (PDIM) from *Mycobacterium tuberculosis* grown in vitro: implications for virulence studies. Microbiology 155:3532–3543. https://doi.org/10.1099/mic.0.029199-0
32. Ford CB, Shah RR, Maeda MK, Gagneux S, Murray MB, Cohen T, Johnston JC, Gardy J, Lipsitch M, Fortune SM. 2013. *Mycobacterium tuberculosis* mutation rate estimates from different lineages predict substantial differences in the emergence of drug resistant tuberculosis. Nat Genet 45:784–790. https://doi.org/10.1038/ng.2656
33. Khader SA, Bell GK, Pearl JE, Fountain JJ, Rangel-Moreno J, Cilley GE, Shen F, Eaton SM, Gaffen SL, Swain SL, Locksley RM, Haynes L, Randall TD, Cooper AM. 2007. IL-23 and IL-17 in the establishment of protective pulmonary CD4+ T cell responses after vaccination and during *Mycobacterium tuberculosis* challenge. Nat Immunol 8:369–377. https://doi.org/10.1038/ni1449
34. Esaulova E, Das S, Singh DK, Choreño-Parra JA, Swain A, Arthur L, Rangel-Moreno J, Ahmed M, Singh B, Gupta A, Fernández-López LA, de la Luz Garcia-Hernandez M, Bucsan A, Moodley C, Mehra S, García-Latorre E, Zuniga J, Atkinson J, Kaushal D, Artyomov MN, Khader SA. 2021. The immune landscape in tuberculosis reveals populations linked to disease

and latency. Cell Host Microbe 29:165–178. https://doi.org/10.1016/j.chom.2020.11.013
35. Lun ATL, McCarthy DJ, Marioni JC. 2016. A step-by-step workflow for low-level analysis of single-cell RNA-seq data with bioconductor. F1000Res 5:2122. https://doi.org/10.12688/f1000research.9501.2
36. Korotkevich G, Sukhov V, Budin N, Shpak B, Artyomov MN, Sergushichev A. 2021. *Fast Gene Set Enrichment Analysis*. Available from: bioRxiv https://doi.org/10.1101/060012